

# Comparative study between discrete and continuum models for the evolution of competing phenotype-structured cell populations in dynamical environments

Aleksandra Ardaševa,<sup>\*</sup> Helen M. Byrne, and Philip K. Maini  
*Wolfson Centre for Mathematical Biology, University of Oxford, UK*

Robert A. Gatenby and Alexander R. A. Anderson  
*Department of Integrated Mathematical Oncology, H. Lee Moffitt Cancer Center, USA*

Tommaso Lorenzi<sup>†</sup>  
*Department of Mathematical Sciences “G. L. Lagrange”,  
Dipartimento di Eccellenza 2018-2022, Politecnico di Torino, IT*  
(Dated: August 18, 2020)

Deterministic continuum models formulated as non-local partial differential equations for the evolutionary dynamics of populations structured by phenotypic traits have been used recently to address open questions concerning the adaptation of asexual species to periodically fluctuating environmental conditions. These models are usually defined on the basis of population-scale phenomenological assumptions and cannot capture adaptive phenomena that are driven by stochastic variability in the evolutionary paths of single individuals. In light of these considerations, in this paper we develop a stochastic individual-based model for the coevolution of two competing phenotype-structured cell populations that are exposed to time-varying nutrient levels and undergo spontaneous, heritable phenotypic changes with different probabilities. Here, the evolution of every cell is described by a set of rules that result in a discrete-time branching random walk on the space of phenotypic states, and nutrient levels are governed by a difference equation in which a sink term models nutrient consumption by the cells. We formally show that the deterministic continuum counterpart of this model comprises a system of non-local partial differential equations for the cell population density functions coupled with an ordinary differential equation for the nutrient concentration. We compare the individual-based model and its continuum analogue, focussing on scenarios whereby the predictions of the two models differ. The results obtained clarify the conditions under which significant differences between the two models can emerge due to bottleneck effects that bring about both lower regularity of the density functions of the two populations and more pronounced demographic stochasticity. In particular, bottleneck effects emerge in the presence of lower probabilities of phenotypic variation, and are more apparent when the two populations are characterised by lower fitness initial mean phenotypes and smaller initial levels of phenotypic heterogeneity. The emergence of these effects, and thus the agreement between the two modelling approaches, is also dependent on the initial proportions of the two populations. As an illustrative example, we demonstrate the implications of these results in the context of the mathematical modelling of the early stage of metastatic colonisation of distant organs.

## I. INTRODUCTION

Adaptation to dynamically changing environments occurs in a variety of biological and ecological contexts [1–4]. In particular, when changes in nutrient availability occur, individuals in a population can either adopt a highly plastic phenotype [5], which enables them to acquire different traits based on environmental cues, or a risk-spreading strategy (*e.g.* bet-hedging), which allows at least some fraction of the population to survive in the face of sudden environmental changes by producing offspring adapted to the new conditions [6–8].

Mathematical modelling of evolutionary dynamics in time-varying environments has received considerable attention from mathematicians and physicists over the

past fifty years – see, for instance, [9–20] and references therein. Recently, deterministic continuum models formulated in terms of non-local partial differential equations (PDEs) for the evolutionary dynamics of populations, structured by phenotypic traits, have been used to address open questions concerning the adaptation of asexual species to periodically fluctuating environments [21–28].

Although more amenable to analytical and numerical approaches, which allow for a more in-depth theoretical understanding of the underlying dynamics, these deterministic continuum models are usually defined on the basis of population-scale phenomenological assumptions. This makes it more difficult to incorporate the finer details of phenotypic adaptation by single individuals. Moreover, such models cannot capture adaptive phenomena that are driven by stochastic effects in the evolutionary paths of single individuals. This will be particularly relevant at low population levels, which are commonly observed when risk-spreading adaptive strate-

---

<sup>\*</sup> aleksandra.ardaseva@maths.ox.ac.uk

<sup>†</sup> tommaso.lorenzi@polito.it

gies occur [29]. Ideally, we want to derive deterministic continuum models from first principles (*i.e.* as the appropriate limit of discrete stochastic models that track the evolution of single individuals), which permit the representation of individual-scale adaptive mechanisms, and account for possible stochastic inter-individual variability in evolutionary trajectories [30–33].

In light of these considerations, we develop a stochastic individual-based (IB) model for the evolutionary dynamics of two competing phenotype-structured cell populations that are exposed to time-varying nutrient levels and undergo spontaneous, heritable phenotypic changes with different probabilities. In this model, every cell is viewed as an individual agent whose phenotypic state is modelled by a discrete variable, which represents the normalised level of expression of a gene that allows cells to cope with nutrient scarcity. For instance, activation of hypoxia-inducible factors allows mammalian cells to adapt to oxygen deprivation [34]. In the model, cells proliferate, die and undergo phenotypic changes according to a set of rules that correspond to a discrete-time branching random walk on the space of phenotypic states [32, 35]. We assume that the cell proliferation rate depends on nutrient levels, and that nutrient concentration is governed by a difference equation in which a sink term models nutrient consumption by the cells.

This work builds on our earlier analytical and numerical studies of deterministic continuum models for the evolutionary dynamics of competing phenotype-structured asexual populations exposed to periodically-oscillating nutrient levels [22, 23]. In [22], we focussed on a scenario where the evolution of nutrient levels was independent from the dynamics of the populations, and we analysed the long-time behaviour of the solutions to the model equations, in order to dissect the role of spontaneous, heritable phenotypic changes in the adaptation of asexual species to fluctuating environments. In [23], we extended the original model by letting the nutrient levels coevolve with the competing populations and carried out simulation-assisted analysis of the long-time behaviour of the solutions to the model equations in order to investigate how negative feedback mechanisms, which regulate population growth through nutrient consumption, may shape the evolutionary dynamics of cell populations under oscillating environmental conditions. In this paper, we show that the models considered in [22, 23] can be formally obtained as the deterministic continuum limit of the stochastic IB model presented here. Moreover, we conduct a comparative study between the IB model and its continuum analogue, our aim being to explore scenarios in which differences between the outcomes of the two models may emerge.

The paper is organised as follows. In Section II, we introduce the stochastic IB model. In Section III, we present its deterministic continuum counterpart (a formal derivation is provided in Appendix A), which comprises a system of non-local PDEs for the population density functions (*i.e.* the cell distribution over the space of

phenotypic states) coupled with an ordinary differential equation (ODE) for the nutrient concentration. In Section IV, we present the main results of the comparative study between the two models. As an illustrative example, in Section V we interpret our results in the context of the early stage of metastatic colonisation of distant organs by cancer cells. In Section VI, we summarise the main findings and outline directions for future research.

## II. STOCHASTIC INDIVIDUAL-BASED MODEL

We model the evolutionary dynamics of two competing cell populations in a well-mixed system. Cells in the two populations proliferate (*i.e.* divide), die and undergo spontaneous, heritable phenotypic changes. We assume that the two populations differ only in their probability of phenotypic variation. The population undergoing phenotypic changes with a higher probability is labelled by the letter  $H$ , while the other population is labelled by the letter  $L$ . The phenotypic state of every cell at time  $t \in [0, t_f] \subset \mathbb{R}^+$  is characterised by a variable  $x \in [0, 1] \subset \mathbb{R}^+$ , which represents the normalised level of expression of a gene that allows cells to cope with nutrient deprivation. In particular, we assume that cells in the phenotypic state  $x = 0$  are best adapted to nutrient-rich environments, whereas cells in the phenotypic state  $x = 1$  are best adapted to nutrient-scarce environments.

We represent each cell as an agent that occupies a position on a lattice. We discretise the time variable and the phenotypic state via  $t_h = h\tau \in [0, t_f]$  and  $x_j = j\chi \in [0, 1]$ , respectively, where  $h, j \in \mathbb{N}_0$ , and  $\tau \in \mathbb{R}_*^+$  and  $\chi \in \mathbb{R}_*^+$  are the time- and phenotype-step, respectively. We introduce the dependent variable  $N_{i,j}^h \in \mathbb{N}_0$  to represent the number of cells of population  $i \in \{H, L\}$  on lattice site  $j$  (*i.e.* in the  $j^{\text{th}}$  phenotypic state) at time-step  $h$ . The density (*i.e.* the phenotype distribution) of population  $i$ , the size of population  $i$ , and the total number of cells are defined, respectively, as follows

$$n_i(t_h, x_j) = n_{i,j}^h := N_{i,j}^h \chi^{-1}, \quad (1)$$

$$\rho_i(t_h) = \rho_i^h := \sum_j N_{i,j}^h \quad \text{and} \quad \rho(t_h) = \rho^h := \sum_i \rho_i^h. \quad (2)$$

We further define the mean phenotype of population  $i$  and the related standard deviation, respectively, as

$$\mu_i(t_h) = \mu_i^h := \frac{1}{\rho_i^h} \sum_j x_j N_{i,j}^h \quad (3)$$

and

$$\sigma_i(t_h) = \sigma_i^h := \left( \frac{1}{\rho_i^h} \sum_j x_j^2 N_{i,j}^h - (\mu_i^h)^2 \right)^{\frac{1}{2}}. \quad (4)$$

Finally, the nutrient concentration at time-step  $h$  is modelled by the discrete, non-negative function  $S(t_h) = S^h$ .

### A. Mathematical modelling of phenotypic changes

We account for spontaneous, heritable phenotypic changes by allowing cells to update their phenotypic states according to a random walk. More precisely, between the time-steps  $h$  and  $h+1$ , every cell in population  $i \in \{H, L\}$  either enters a new phenotypic state, with probability  $\lambda_i \in [0, 1]$ , or remains in its current phenotypic state, with probability  $1 - \lambda_i$ . Since we assume that phenotypic changes occur randomly due to non-genetic instability, rather than selective pressures [36], then a cell of population  $i$  in phenotypic state  $x_j$  that undergoes a phenotypic change enters into either of the phenotypic states  $x_{j \pm 1} = x_j \pm \chi$  with probabilities  $\lambda_i/2$ . No-flux boundary conditions are implemented by aborting any attempted phenotypic variation of a cell if it requires moving into a phenotypic state outside the interval  $[0, 1]$ .

### B. Mathematical modelling of cell division and death

Cells divide, die or remain quiescent with probabilities that depend on their phenotypic states, the total number of cells and the nutrient concentration. We assume that a dividing cell is replaced by two identical cells that inherit the phenotypic state of the parent cell (*i.e.* the progenies are placed on the same lattice site as their parent), while a dying cell is removed from the population.

In order to translate into mathematical terms the idea that larger population sizes correspond to more intense competition between cells, at every time-step  $h$  we allow cells to die due to intra-population and inter-population competition at a rate proportional to the total cell number  $\rho^h$ , with constant of proportionality  $d > 0$ .

We denote by  $p(x_j, S^h)$  the division rate of a cell in the  $j^{th}$  phenotypic state, where  $S^h$  is the nutrient concentration. Since  $x_j$  represents the normalised expression level of a gene that allows cells to cope with nutrient scarcity, we assume that phenotypic variants with  $x_j \rightarrow 0$  are characterised by the maximal division rate when nutrient is abundant (*i.e.* if  $S^h \rightarrow \infty$ ), whereas phenotypic variants with  $x_j \rightarrow 1$  are characterised by the maximal division rate when nutrient is scarce (*i.e.* if  $S^h \rightarrow 0$ ). Our implicit assumption here is that cells in the phenotypic state  $x_j = 1$  switch to other nutrients that are abundant, and therefore they are no longer dependent on the specific nutrient we are modelling. (We refer the interested reader to Section V for a specific biological application of this modelling approach). Under these assumptions, and following the modelling strategies that we proposed in [22, 23], we define the cell division rate  $p(x_j, S^h)$  as

follows

$$p(x_j, S^h) := \gamma \frac{S^h}{\kappa + S^h} (1 - x_j^2) + \zeta \left( 1 - \frac{S^h}{\kappa + S^h} \right) [1 - (1 - x_j)^2]. \quad (5)$$

In Eq. (5), the parameters  $\gamma > 0$  and  $\zeta > 0$  model, respectively, the maximum cell division rate of the phenotypic variants best adapted to nutrient-rich and nutrient-scarce environments (*i.e.* cells in the phenotypic states  $x_j = 0$  and  $x_j = 1$ , respectively). To incorporate into the model the possible fitness cost associated with the ability to survive in nutrient-scarce environments [37, 38], we make the additional assumption that  $\zeta \leq \gamma$ . Moreover,  $\kappa > 0$  is the Michaelis constant of the nutrient, *i.e.* the nutrient concentration at which the proliferation rate is half maximal. After a little algebra, Eq. (5) can be rewritten as

$$p(x_j, S^h) = \gamma g(S^h) - h(S^h)(x_j - \varphi(S^h))^2, \quad (6)$$

where

$$g(S^h) := \frac{S^h}{\kappa + S^h} + \frac{\zeta^2 \kappa^2}{\gamma(\kappa + S^h)(\gamma S^h + \zeta \kappa)},$$

$$\varphi(S^h) := \frac{\zeta \kappa}{\gamma S^h + \zeta \kappa} \quad \text{and} \quad h(S^h) := \frac{\gamma S^h + \zeta \kappa}{\kappa + S^h}. \quad (7)$$

Here,  $\gamma g(S^h)$  is the maximum fitness,  $\varphi(S^h)$  is the fittest phenotypic state and  $h(S^h)$  is a selection gradient. Consistent with our modelling assumptions, we have

$$\varphi : [0, \infty) \rightarrow [0, 1], \quad \lim_{S \rightarrow 0} \varphi(S) = 1 \quad \text{and} \quad \lim_{S \rightarrow \infty} \varphi(S) = 0.$$

Under these assumptions, between time-steps  $h$  and  $h+1$ , a cell in the  $j^{th}$  phenotypic state may divide with probability

$$\mathcal{P}_b := \tau p(x_j, S^h), \quad (8)$$

die with probability

$$\mathcal{P}_d := \tau d \rho^h, \quad (9)$$

or remain quiescent (*i.e.* do not divide nor die) with probability

$$\mathcal{P}_q := 1 - \tau (p(x_j, S^h) + d \rho^h). \quad (10)$$

Notice that we are implicitly assuming that the time-step  $\tau$  is sufficiently small that  $0 < \mathcal{P}_i < 1$  for all  $i \in \{b, d, q\}$ .

### C. Mathematical modelling of nutrient dynamics

Following Ardaševa *et al.* [23], we describe the nutrient dynamics via the following difference equation for  $S^h$

$$S^{h+1} = S^h + \tau \left[ I^h - \eta S^h - \theta \gamma \frac{S^h}{\kappa + S^h} \sum_j (1 - x_j)^2 (N_{H,j}^h + N_{L,j}^h) \right], \quad (11)$$

complemented with a suitable initial nutrient concentration  $S^0$ . Since we consider a well-mixed system, there is no diffusion of the nutrient. In the difference equation (11), the parameter  $\eta > 0$  represents the rate of natural decay of the nutrient, while the last term on the right-hand side of the difference equation (11) models the rate of nutrient consumption by the cells and is based on the following argument. Cells in the phenotypic state  $x_j = 1$  do not rely on the nutrient we are modelling for their survival – these cells might produce energy via different metabolic pathways that do not require the nutrient under consideration – and, as such, they do not consume any nutrient. By contrast, cells in the phenotypic state  $x_j = 0$  consume the nutrient at a rate proportional to their cell division rate, with constant of proportionality  $\theta > 0$ . Finally, the rate at which the nutrient is consumed by cells in phenotypic states  $x_j \in (0, 1)$  is a fraction of the consumption rate of cells in the phenotypic state  $x_j = 0$ , with higher values of  $x_j$  correlating with lower rates of nutrient consumption. The discrete, non-negative function  $I^h$  on the right-hand side of the difference equation (11) models the rate at which the nutrient is supplied to the system. When the nutrient inflow is constant we fix

$$I^h \equiv \bar{I} \geq 0; \quad (12)$$

when the nutrient inflow undergoes periodic oscillations we prescribe

$$I^h := \max \left( 0, A \sin \left( \frac{2\pi t_h}{T} \right) \right), \quad (13)$$

with the parameters  $T > 0$  and  $A > 0$  modelling, respectively, the period and the amplitude of the oscillations.

### D. Computational implementation

Numerical simulations of the IB model are performed using the open-source Java library **Hybrid Automata Library (HAL)** [39]. At each time-step, we follow the procedures summarised in Figure 1 and described hereafter to simulate phenotypic changes as well as cell division and death. All random numbers mentioned below are real numbers drawn from the standard uniform distribution on the interval  $(0, 1)$  using the Java function `Rand.Double()`.

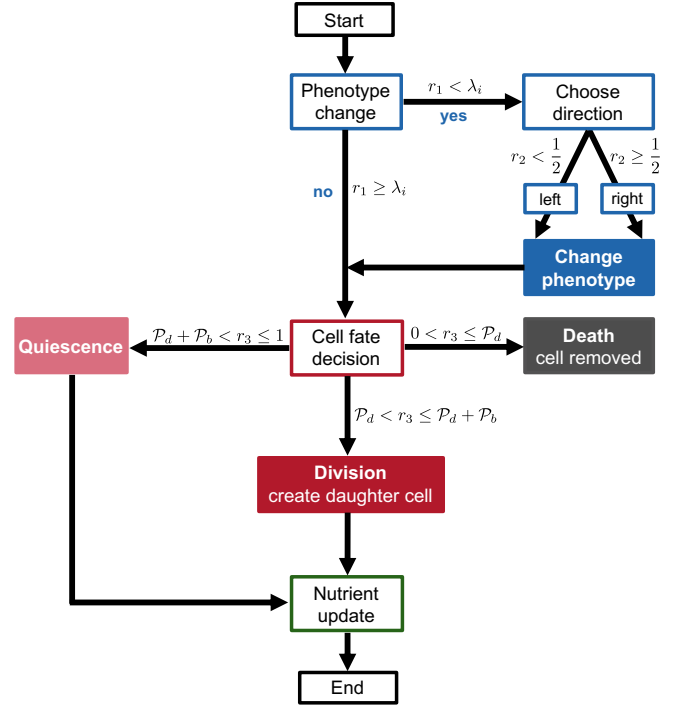


FIG. 1. Flowchart illustrating the procedure underlying the computational implementation of the stochastic IB model for each cell at every time-step. Once all cells have undergone both the phenotype-change step and the fate-decision step, the total number of cells is computed and the nutrient level is updated.

*a. Computational implementation of spontaneous, heritable phenotypic changes.* For each cell in population  $i$ , a random number,  $r_1$ , is generated and used to determine whether the cell undergoes a phenotypic change (*i.e.*  $0 < r_1 < \lambda_i$ ) or not (*i.e.*  $\lambda_i \leq r_1 < 1$ ). If the cell undergoes a phenotypic change, then a second random number,  $r_2$ , is generated. If  $0 < r_2 < 1/2$ , then the cell moves into the phenotypic state to the left of its current state, *i.e.* a cell in the phenotypic state  $x_j$  will move into the phenotypic state  $x_{j-1} = x_j - \chi$ , whereas if  $1/2 \leq r_2 < 1$  then the cell moves into the phenotypic state to the right of its current state, *i.e.* a cell in the phenotypic state  $x_j$  will move into the phenotypic state  $x_{j+1} = x_j + \chi$ . No-flux boundary conditions are implemented by aborting attempted phenotypic changes that would move a cell into a phenotypic state outside the unit interval.

*b. Computational implementation of cell division and death.* For each population, the number of cells in each phenotypic state is counted. The size of each cell population and the total number of cells are then computed via Eq. (2). Definitions (8)–(10) are used to

calculate the probabilities of cell division, death and quiescence for every phenotypic state. For each cell, a random number,  $r_3$ , is generated and the cells' fate is determined by comparing this number with the probabilities of division, death and quiescence corresponding to the phenotypic state of the cell. If  $0 < r_3 < \mathcal{P}_d$  then the cell is considered dead and is removed from the population. If  $\mathcal{P}_d \leq r_3 < \mathcal{P}_d + \mathcal{P}_b$  then the cell undergoes division and an identical daughter cell is created. Finally, if  $\mathcal{P}_d + \mathcal{P}_b \leq r_3 < 1$  then the cell remains quiescent (*i.e.* does not divide nor die).

*c. Computational implementation of nutrient dynamic.* At each time-step, the number of cells of the two populations in each phenotypic state is counted in order to evaluate the last term on the right-hand side of the difference equation (11). The nutrient concentration is then updated via the difference equation (11).

### III. CORRESPONDING DETERMINISTIC CONTINUUM MODEL

Using the formal method presented in [32, 33], we let the time-step  $\tau \rightarrow 0$  and the phenotype-step  $\chi \rightarrow 0$  in such a way that

$$\frac{\lambda_i \chi^2}{2\tau} \rightarrow \beta_i \in \mathbb{R}_*^+ \quad \text{for } i \in \{H, L\}. \quad (14)$$

Here, the parameter  $\beta_i$  is the rate of spontaneous, heritable phenotypic changes of cells in population  $i$ . It is then possible to formally show (see Appendix A) that the deterministic continuum counterpart of the stochastic IB model is given by the following system of non-local PDEs for the cell population density functions  $n_H(x, t)$  and  $n_L(x, t)$

$$\begin{cases} \frac{\partial n_H}{\partial t} = \beta_H \frac{\partial^2 n_H}{\partial x^2} + (p(x, S(t)) - d\rho(t))n_H, \\ \frac{\partial n_L}{\partial t} = \beta_L \frac{\partial^2 n_L}{\partial x^2} + (p(x, S(t)) - d\rho(t))n_L, \\ \rho(t) := \rho_H(t) + \rho_L(t), \quad \rho_i(t) := \int_0^1 n_i(x, t) dx, \end{cases} \quad (15)$$

posed on  $(0, 1) \times (0, t_f]$  and subject to no-flux boundary conditions, *i.e.*

$$\frac{\partial n_i(0, t)}{\partial x} = 0, \quad \frac{\partial n_i(1, t)}{\partial x} = 0 \quad \text{for all } t \in (0, t_f]. \quad (16)$$

In the system of non-local PDEs (15), the nutrient concentration  $S(t)$  is governed by the continuum counterpart of the difference equation (11), *i.e.* the following ODE

posed on  $(0, t_f]$

$$\frac{dS}{dt} = I(t) - \eta S - \theta \gamma \frac{S}{\kappa + S} \int_0^1 (1-x^2) (n_H + n_L) dx, \quad (17)$$

which can be easily obtained in a formal way by letting  $\tau \rightarrow 0$  and  $h \rightarrow 0$  in the ODE (11). In the continuum modelling framework given by the system of non-local PDEs (15), the mean phenotype of population  $i$  and the related standard deviation are defined, respectively, as

$$\mu_i(t) := \frac{1}{\rho_i(t)} \int_0^1 x n_i(x, t) dx \quad (18)$$

and

$$\sigma_i(t) := \left( \frac{1}{\rho_i(t)} \int_0^1 x^2 n_i(x, t) dx - \mu_i^2(t) \right)^{\frac{1}{2}}, \quad (19)$$

for  $i \in \{H, L\}$ .

### IV. MAIN RESULTS

In this section, we compare the results of numerical simulations of the stochastic IB model introduced in Section II and numerical solutions of the corresponding deterministic continuum model presented in Section III.

For consistency with previous mathematical studies of the evolutionary dynamics of phenotype-structured populations, which rely on the *prima facie* assumption that population densities are Gaussians [40], simulations are carried out under the assumption that the initial phenotype distribution of population  $i$  for the IB model is of the form

$$n_{i,j}^0 = a_i \left( \frac{b}{2\pi} \right)^{\frac{1}{2}} \exp \left[ -\frac{b}{2} (x_j - c)^2 \right], \quad (20)$$

with  $i \in \{H, L\}$ . In Eq. (20), the parameter  $a_i$  is related to the initial size of population  $i$ , while the parameters  $b$  and  $c$  are related, respectively, to the inverse of the initial standard deviation and the initial mean phenotype of the two populations. The initial population density  $n_i(x, 0)$  for the continuum model is defined as the continuum analogue of Eq. (20) (see Appendix B).

First, we present a sample of base-case results that demonstrate excellent quantitative agreement between the stochastic IB model and its deterministic continuum counterpart. Then, we perform a systematic sensitivity analysis of some key parameters. In particular, we investigate how the base-case results change as we vary the values of the probabilities of phenotypic variation  $\lambda_H$  and  $\lambda_L$  (see Section IV B), the parameters  $b$  and  $c$  in Eq. (20) (see Section IV C) – *i.e.* the inverse of the initial standard deviation and the initial mean phenotype of the two populations – and the parameters  $a_H$  and  $a_L$  in Eq. (20) (see Section IV D) – *i.e.* the initial sizes of

TABLE I. Parameter values used in numerical simulations.

	Description	Values
$\lambda_H$	Probability of phenotypic variation of population $H$	$\{0.05, 0.4, 1\}$
$\lambda_L$	Probability of phenotypic variation of population $L$	$\{0.02, 0.2\}$
$\gamma$	Maximum cell division rate of phenotypic variants $x = 0$	100
$\zeta$	Maximum cell division rate of phenotypic variants $x = 1$	50
$\kappa$	Michaelis constant of nutrient	1
$d$	Death rate due to inter- and intra-population competition	$\{0.01, 0.1, 0.2, 0.4, 1.0\}$
$\theta$	Consumption rate of nutrient	$\{10^{-5}, 10^{-4}, 2 \times 10^{-4}, 10^{-3}\}$
$\eta$	Rate of natural decay of nutrient	$10^{-3}$
$S^0$	Initial nutrient concentration	$\{0, 10\}$
$a_i$	Initial size of population $i$	800
$c$	Initial mean phenotype of both populations	$\{0, 0.5, 1\}$
$b$	Initial inverse variance of both populations	$\{10, 1000\}$
$\bar{I}$	Constant rate of oxygen supply	10
$A$	Amplitude of fluctuations in oxygen supply	$\{30, 200\}$
$T$	Period of fluctuations in oxygen supply	5
$\varepsilon$	Scaling factor for the rate of phenotypic variation (Section IV B)	$\{1, 2, \dots, 10\}$
$\nu$	Initial proportion of population $H$ (Section IV D)	$\{0.1, 0.2, 0.3, 0.7, 0.8, 0.9\}$
$Z$	Initial total number of cells (Section IV D)	800
$\chi$	Phenotype-step	0.032
$\tau$	Time-step	$10^{-3}$
$t_f$	Final time	$\{10, 20, 40\}$

the two populations.

We consider the nutrient concentration to be non-dimensionalised and use the dimensionless parameter values listed in Table I to carry out numerical simulations of the IB model. The methods employed to numerically solve the equations of the related continuum model are described in Appendix B.

#### A. Base-case results

We first assume that the supply rate of nutrient is constant (*i.e.* we define the term  $I^h$  via Eq. (12)) and consider different values of the nutrient consumption rate  $\theta$ . The results displayed in Figure 2 show excellent quantitative agreement between numerical simulations of the IB and continuum models, both for relatively low and relatively high values of  $\theta$ . As expected, based on the results we presented in [23], population  $L$  outcompetes population  $H$ , which eventually goes extinct. Moreover, since the nutrient concentration converges to smaller equilibrium values for larger values of the nutrient consumption rate, higher values of  $\theta$  correspond to decreasing equilibrium sizes of population  $L$  and equilibrium values of the mean phenotype which are closer to 1 (*i.e.* the fittest phenotypic state in nutrient-scarce environments). In all cases, the phenotype distribution of the surviving population is unimodal and attains its maximum at the mean phenotype (see Figures 10(a) and 10(b) in Appendix C).

We then let the supply rate of nutrient undergo periodic oscillations (*i.e.* we define the term  $I^h$  via Eq. (13))

and, informed by numerical results presented in [23], we consider different values of the consumption rate  $\theta$  that lead to the emergence of either mild (*i.e.* small-amplitude) or severe (*i.e.* large-amplitude) fluctuations in the nutrient concentration  $S^h$ . The results displayed in Figure 3 demonstrate that, both for mild and severe fluctuations in the nutrient concentration, the size and the mean phenotype of the surviving population converge to positive  $T$ -periodic functions. Furthermore, in agreement with the analytical results we presented in [22], the numerical results in Figure 3 indicate that, when nutrient levels undergo smaller fluctuations, population  $L$  survives (see Figure 3(b)). On the other hand, when nutrient levels undergo larger fluctuations, population  $H$  ultimately outcompetes population  $L$  (see Figure 3(a)). In both cases, the phenotype distribution of the surviving population is unimodal and attains its maximum at the mean phenotype (see Figures 10(c) and 10(d) in Appendix C). Moreover, excellent agreement between numerical simulations of the IB and continuum models is observed.

The numerical results presented in Appendix D show that analogous conclusions hold in the simplified scenario where the concentration of nutrient is prescribed and does not coevolve with the cells.

#### B. Sensitivity analysis of the probabilities of phenotypic variation

Based on the analytical results presented in [22] for a simplified continuum model, we expect smaller values of  $\lambda_H$  and  $\lambda_L$  (*i.e.* the probabilities of phenotypic varia-

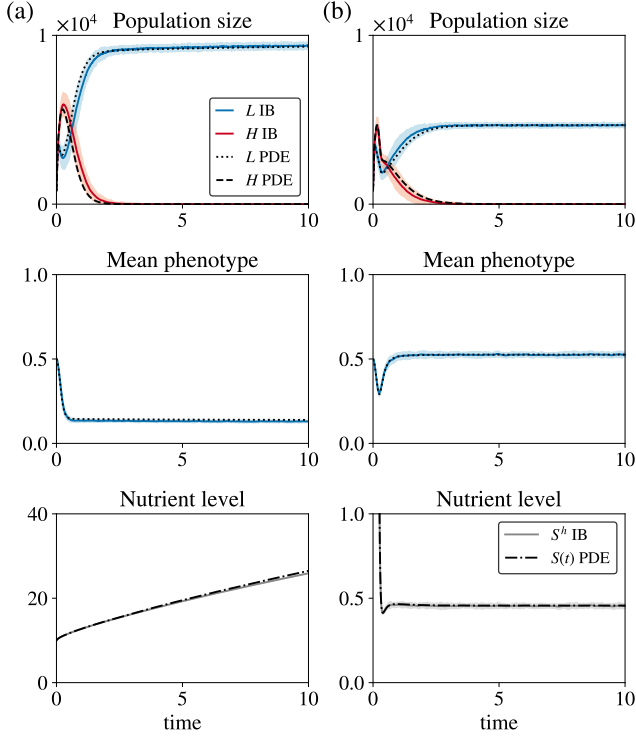


FIG. 2. **Base-case results when the nutrient inflow is constant.** Comparison between numerical simulations of the IB (solid, coloured lines) and continuum (broken, black lines) models in the case where the evolution of the nutrient concentration is governed by the difference equation (11) whereby the term  $I^h$  is defined via Eq. (12) with  $\bar{I} = 10$ . (a) Dynamics of the population sizes (top panel), mean phenotype of the surviving population (central panel) and nutrient level (bottom panel) in the case where  $\theta = 10^{-5}$ . Here,  $a_H = a_L = 800$ ,  $b = 1000$  and  $c = 0.5$  in Eq. (20), and the values of the other parameters are those listed in Table I with  $\lambda_H = 1$  and  $\lambda_L = 0.2$ . The results from the IB model correspond to the average over 30 realisations and the related variance is displayed by the coloured areas surrounding the curves. (b) Same as (a) but for larger nutrient consumption, *i.e.*  $\theta = 10^{-4}$ .

tion) to correlate with longer transient intervals in the dynamics of the sizes of the two cell populations. To test this hypothesis, we focus on the case where the supply rate of nutrient is constant (*i.e.* when the term  $I^h$  is defined via Eq. (12)). We carry out numerical simulations of the IB model assuming

$$\lambda_i = \varepsilon \Lambda_i, \quad (21)$$

with  $\Lambda_i$  fixed and  $\varepsilon \in \{1, \dots, 10\}$ . As summarised by the plots in Figure 4, smaller values of  $\varepsilon$  bring about longer transient intervals (*i.e.* larger values of  $t_{tr}$  in Figure 4(d)) during which the two populations coexist before population  $L$  ultimately out-competes population  $H$ .

The results displayed in Figure 4(a)–(c) indicate that the size of population  $L$  decreases during the transient,

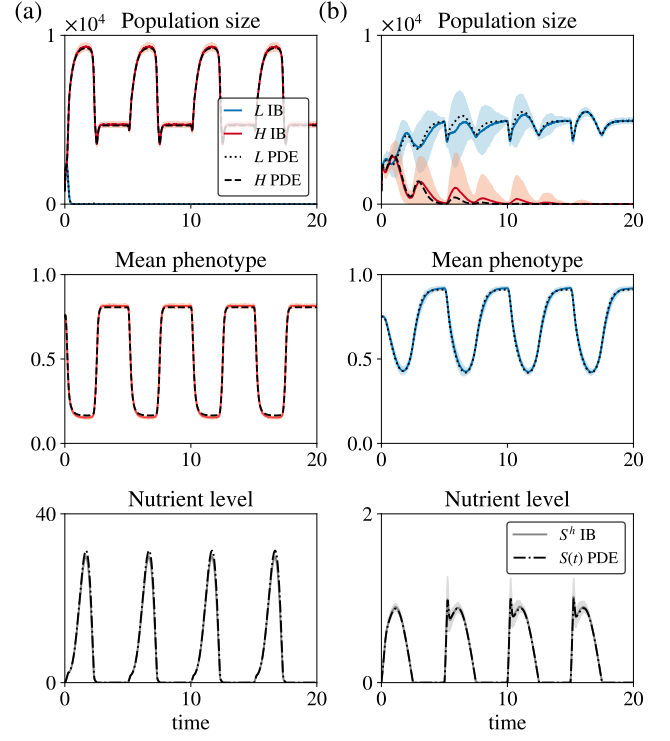


FIG. 3. **Base-case results when the nutrient inflow is periodic.** Comparison between numerical simulations of the IB (solid, coloured lines) and continuum (broken, black lines) models in the case where the evolution of the nutrient concentration is governed by the difference equation (11) whereby the term  $I^h$  is defined via Eq. (13) with  $A = 200$  and  $T = 5$ . (a) Dynamics of the population sizes (top panel), mean phenotype of the surviving population (central panel) and nutrient level (bottom panel) in the case where  $\theta = 2 \times 10^{-4}$ . Here,  $a_H = a_L = 800$ ,  $b = 1000$  and  $c = 0.5$  in Eq. (20), and the values of the other parameters are those listed in Table I with  $\lambda_H = 0.4$  and  $\lambda_L = 0.02$ . The results from the IB model correspond to the average over 30 realisations and the related variance is displayed by the coloured areas surrounding the curves. (b) Same as (a) but for larger nutrient consumption, *i.e.*  $\theta = 10^{-3}$ .

defined as the early part of the population trajectory, before approaching steady-state. Moreover, longer transients correlate with sharper drops in the size of population  $L$ , and thus smaller minimum values of  $\rho_L$  (*i.e.* smaller  $\rho_L^{min}$  in Figure 4(d)), which makes bottleneck effects that bring about both lower regularity of the density functions of the two populations, and more pronounced demographic stochasticity more likely to come into play. This suggests that lower probabilities of phenotypic variation may create conditions for the emergence of differences between predictions of the IB and continuum models.

To investigate this further, we compare numerical simulations of the IB model with numerical solutions of the continuum model in the setting of Figure 2 (*i.e.* defining the nutrient supply term  $I^h$  via Eq. (12) and consider-

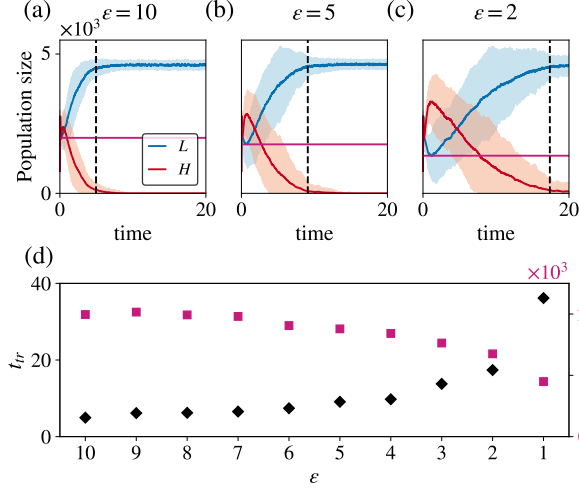


FIG. 4. **Emergence of longer transient intervals for lower probabilities of phenotypic variation.** (a)-(c). Numerical simulations of the IB model in the case where the probabilities of phenotypic variation  $\lambda_H$  and  $\lambda_L$  are defined via Eq. (21) with  $\Lambda_H = 0.05$ ,  $\Lambda_L = 0.02$ , and  $\varepsilon = 10$  (panel (a)) or  $\varepsilon = 5$  (panel (b)) or  $\varepsilon = 2$  (panel (c)). The black dashed lines highlight the time  $t_{tr}$  such that  $\rho_L(t_f) - \rho_L(t_{tr}) < 100$ , while the solid pink lines highlight the value of  $\rho_L^{min} := \min_h \rho_L^h$ . These results correspond to the average over 30 realisations and the related variance is displayed by the coloured areas surrounding the curves. (d). Plots of  $t_{tr}$  (black diamonds) and  $\rho_L^{min}$  (pink squares) as functions of  $\varepsilon \in \{1, \dots, 10\}$ . The evolution of the nutrient concentration is governed by the difference equation (11), whereby the term  $I^h$  is defined via Eq. (12) with  $\bar{I} = 10$ . Here,  $a_H = a_L = 800$ ,  $b = 1000$  and  $c = 0.5$  in Eq. (20), and the values of the other parameters are those listed in Table I with  $\theta = 10^{-3}$ .

ing different values of nutrient consumption rate  $\theta$ ) but using lower values of the probabilities of phenotypic variation  $\lambda_H$  and  $\lambda_L$ . The results, summarised in Figure 5, demonstrate that while excellent quantitative agreement between numerical simulations of the IB model and numerical solutions of the continuum model is obtained for relatively large values of  $\theta$  (see Figure 5(b)), significant differences in the behaviour of the two models can be observed for relatively low values of  $\theta$  (see Figure 5(a)). Such differences persist when smaller values of the time-step  $\tau$  and the phenotype-step  $\chi$  are considered. More specifically, lower time- and phenotype-steps correlate with a more drastic decay in the size of population  $L$ , which then becomes more prone to extinction due to demographic stochasticity.

This is because, when lower values of  $\lambda_H$  and  $\lambda_L$  are considered, a relatively small nutrient consumption rate  $\theta$  corresponds to a longer initial phase of cell dynamics during which the size of population  $L$  decays and the size of population  $H$  grows. After this initial phase, the numerical solutions of the continuum model exhibit trend inversion, with the size of population  $L$  converging to a stable

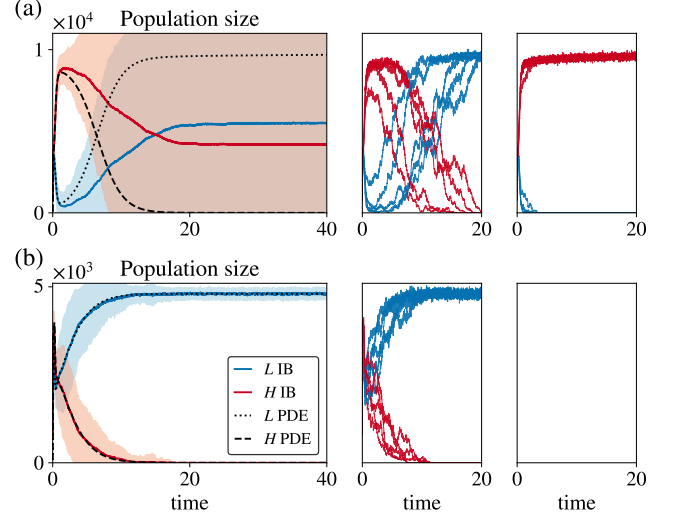


FIG. 5. **Sensitivity analysis of the probabilities of phenotypic variation.** (a) Comparison between numerical simulations of the IB (solid, coloured lines in the left panel) and continuum (broken, black lines in the left panel) models under the parameter setting of Figure 2(a) but with  $\lambda_H = 0.05$  and  $\lambda_L = 0.02$ . The results from the IB model correspond to the average over 30 realisations and the related variance is displayed by the coloured areas surrounding the curves. The plots in the central and right panels show the dynamics of the sizes of the two populations for single realisations of the IB model that match with (central panel) or differ from (right panel) numerical solutions of the continuum model. (b) Same as (a) for the parameter setting of Figure 2(b) but with  $\lambda_H = 0.05$  and  $\lambda_L = 0.02$ .

positive value and the size of population  $H$  decaying to zero. Numerical simulations of the IB model, however, demonstrate that there are realisations whereby, due to stochastic effects, the aftermath of the initial phase of cell dynamics is the extinction of population  $L$  and the survival of population  $H$  (see right panel of Figure 5(a)).

Differences between the discrete and the continuum models are also observed when the supply rate of nutrient undergoes periodic oscillations (*i.e.* when the term  $I^h$  is defined via Eq. (13)) and different values of  $\theta$  are considered, provided that lower values of  $\lambda_H$  and  $\lambda_L$  are chosen (results not shown). In this case, for values of nutrient consumption rate  $\theta$  leading to the emergence of severe fluctuations in the nutrient level (*i.e.* when population  $H$  is ultimately selected according to the continuum model), there is an excellent quantitative agreement between the two models. On the other hand, for values of  $\theta$  leading to the emergence of mild fluctuations in nutrient levels (*i.e.* when the continuum model predicts that population  $L$  will ultimately be selected after an initial phase of population size contraction), there are realisations of the IB model in which population  $L$  is outcompeted by population  $H$ .



### C. Sensitivity analysis of the initial standard deviation and the initial mean phenotype

Based on analytical results presented in [22] for a simplified continuum model, in the case where the nutrient concentration coevolves with the cells according to the difference equation (11) and the supply rate  $I^h$  is defined via Eq. (12), we anticipate stronger bottleneck effects in the presence of both small initial standard deviations,  $\sigma_{H,L}^0$ , and large distances between the initial mean phenotypes,  $\mu_{H,L}^0$ , and the equilibrium value of the fittest phenotypic state,  $\varphi(S^\infty)$ , which is computed by substituting the long-time limit  $S^\infty$  of the nutrient concentration into Eq. (7). Since the results presented in Section IV B demonstrate that stronger bottleneck effects may promote the emergence of differences between the predictions of the two models, we expect that larger values of  $|\mu_H^0 - \varphi(S^\infty)|$  and  $|\mu_L^0 - \varphi(S^\infty)|$ , along with smaller values of  $\sigma_H^0$  and  $\sigma_L^0$ , will increase the likelihood of observing differences between numerical simulations of the IB and continuum models.

To test this hypothesis, we first suppose the nutrient supply rate to be constant and we carry out numerical simulations for different values of the parameters  $b$  and  $c$  in Eq. (20). We recall that larger values of  $b$  correlate with lower  $\sigma_H^0$  and  $\sigma_L^0$ ; moreover, in the setting considered here, lower values of  $c$  correspond to higher  $|\mu_H^0 - \varphi(S^\infty)|$  and  $|\mu_L^0 - \varphi(S^\infty)|$  (*i.e.* less fit initial mean phenotypes). The plots presented in Figure 6(a) reveal excellent quantitative agreement between numerical simulations of the IB and continuum models for sufficiently large values of  $\sigma_H^0$  and  $\sigma_L^0$ , regardless of the values of  $|\mu_H^0 - \varphi(S^\infty)|$  and  $|\mu_L^0 - \varphi(S^\infty)|$  (*i.e.* independently of the value of  $c$ ). On the other hand, and consistent with our expectations, the numerical results presented in Figure 6(b) show that, for sufficiently small values of  $\sigma_H^0$  and  $\sigma_L^0$ , higher  $|\mu_H^0 - \varphi(S^\infty)|$  and  $|\mu_L^0 - \varphi(S^\infty)|$  (*i.e.* lower values of  $c$ ) correlate with stronger bottleneck effects leading to the emergence of differences between the cell dynamics produced by the two models.

We now suppose that the nutrient supply rate undergoes periodic oscillations and perform numerical simulations for different values of the parameter  $c$  (*i.e.* the initial mean phenotype of the two populations), which correspond to different values of the quantities  $|\mu_H^0 - \langle \varphi \rangle|$  and  $|\mu_L^0 - \langle \varphi \rangle|$ , where

$$\langle \varphi \rangle := \frac{1}{2} \left( \min_{t_h \in [0, T]} \tilde{S}(t^h) + \max_{t_h \in [0, T]} \tilde{S}(t^h) \right) \quad (22)$$

with  $\tilde{S}(t^h) = \tilde{S}^h$  being the positive  $T$ -periodic function to which  $S^h$  converges as  $h \rightarrow \infty$ . In the setting considered here, smaller values of  $c$  correspond to higher  $|\mu_H^0 - \langle \varphi \rangle|$  and  $|\mu_L^0 - \langle \varphi \rangle|$  (*i.e.* less fit initial mean phenotypes). The results presented in Figure 7(b) indicate that excellent quantitative agreement is observed between numerical simulations of the IB and continuum models when the consumption rate  $\theta$  is such that the

nutrient level undergoes severe fluctuations (*i.e.* when population  $H$  is ultimately selected according to the continuum model), regardless of the values of  $|\mu_H^0 - \langle \varphi \rangle|$  and  $|\mu_L^0 - \langle \varphi \rangle|$  (*i.e.* independently of the value of  $c$ ). On the other hand, the results presented in Figure 7(a) show that, when  $\theta$  is such that the nutrient level undergoes mild fluctuations (*i.e.* when the continuum model predicts population  $L$  to be ultimately selected after an initial phase of population size contraction), good quantitative agreement between numerical simulations of the IB and continuum models is observed only if  $|\mu_L^0 - \langle \varphi \rangle|$  and  $|\mu_H^0 - \langle \varphi \rangle|$  are sufficiently small (*i.e.* only if  $c$  is sufficiently large). Indeed, larger values of these distances correlate with stronger bottleneck effects that may drive discrepancies between the cell dynamics of the two models.

### D. Sensitivity analysis of the initial population sizes

Motivated by the numerical results presented in Section IV C, we hypothesise that differences between numerical simulations of the IB and continuum models, which are observed for sufficiently large values of  $|\mu_i^0 - \varphi(S^\infty)|$  (*i.e.* sufficiently small  $c$ ) and sufficiently small values of  $\sigma_i^0$  (*i.e.* sufficiently high  $b$ ), will be amplified when smaller initial sizes of population  $L$  are considered and the initial total number of cells is held fixed. Indeed, lower values of  $\rho_L^0$  may exaggerate stochastic effects associated with small population sizes in the course of the population bottleneck that occurs in the initial phase of the cell dynamics (*i.e.* when the size of population  $L$  decays). To test this hypothesis, we focus on the case where the nutrient inflow rate is constant and carry out numerical simulations for which the parameters  $a_H$  and  $a_L$  (*i.e.* the parameters linked to the initial population sizes) in Eq. (20) are related as follows

$$a_H = \nu Z \quad \text{and} \quad a_L = (1 - \nu)Z, \quad (23)$$

with  $Z$  fixed and for increasing values of  $0 < \nu < 1$ .

The results presented in Figure 8 show that, higher values of  $\nu$  lead to a sharper bottleneck in population  $L$  and longer transient intervals during which the two populations coexist. For all admissible values of  $\nu$ , the solutions of the continuum model are such that the size of population  $L$  evolves to a stable positive value and population  $H$  becomes extinct. By contrast, for  $\nu$  sufficiently large there are realisations of the IB model whereby population  $H$  outcompetes population  $L$ . Moreover, the size of population  $H$  may undergo small stochastic fluctuations about a stable positive value that is larger than that about which the size of population  $L$  fluctuates – *i.e.* the mean size of population  $H$  is larger than the mean size of population  $L$ .

Analogous results pertain when a periodic nutrient inflow defined via Eq. (13) is considered, provided that

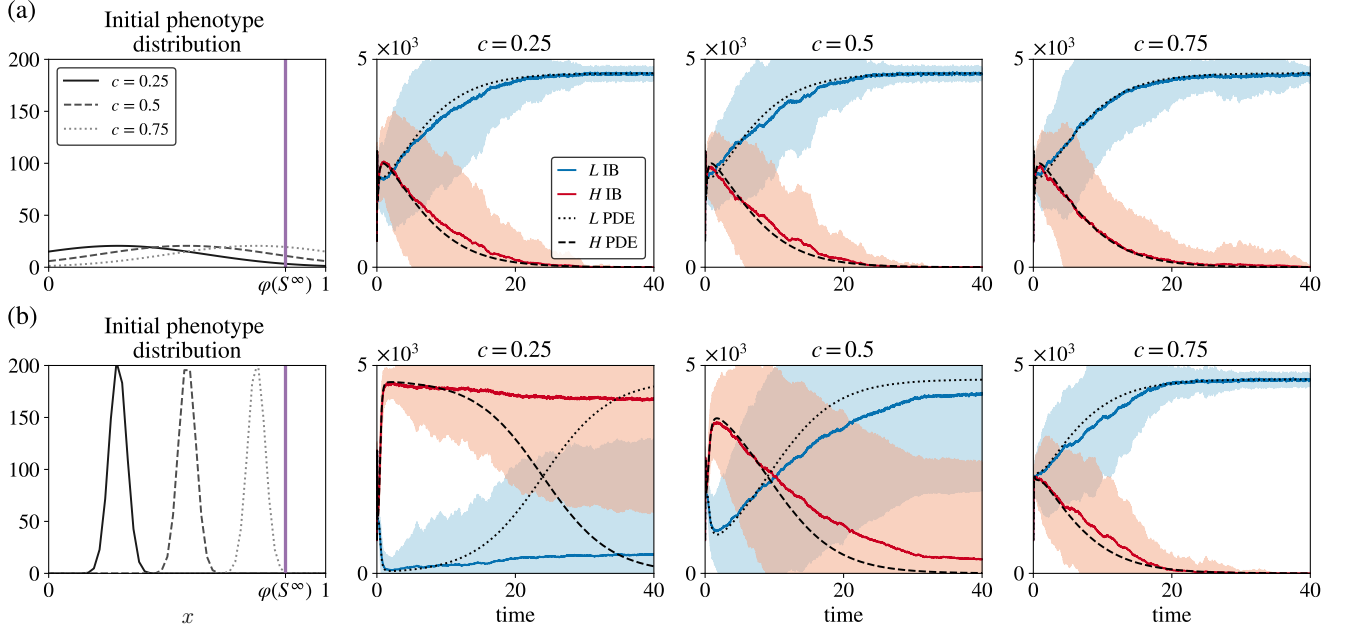


FIG. 6. **Sensitivity analysis of the initial mean phenotype and the initial standard deviation when the nutrient inflow is constant.** (a) Comparison between numerical simulations of the IB (solid, coloured lines in panels 2–4) and continuum (broken, black lines in panels 2–4) models in the case where the initial phenotype distributions of the two populations are defined as shown by the plots in the first panel, corresponding to different values of  $c$  in Eq. (20). The purple line in the first panel highlights the equilibrium value of the fittest phenotypic state  $\varphi(S^\infty)$ , which is computed by substituting into Eq. (7) the long-time limit  $S^\infty$ . The evolution of  $S^h$  is governed by the difference equation (11), whereby the term  $I^h$  is defined via Eq. (12) with  $\bar{I} = 10$ . Here,  $a_H = a_L = 800$  and  $b = 10$  in Eq. (20), and the values of the other parameters are those listed in Table I with  $\lambda_H = 0.05$ ,  $\lambda_L = 0.02$  and  $\theta = 10^{-3}$ . The results from the IB model correspond to the average over 30 realisations and the related variance is displayed by the coloured areas surrounding the curves. (b) Same as (a) but for  $b = 1000$ .

values of  $\theta$  leading to the emergence of mild fluctuations in the nutrient level are chosen (*i.e.* when the continuum model predicts population  $L$  to be ultimately selected after an initial phase of population size contraction) along with sufficiently high  $|\mu_L^0 - \langle \varphi \rangle|$  and  $|\mu_H^0 - \langle \varphi \rangle|$  (results not shown).

## V. APPLICATION TO THE MATHEMATICAL MODELLING OF METASTATIC COLONISATION

The results presented in Section IV lead us to conclude that significant differences between the predictions made by the stochastic IB model and the corresponding deterministic continuum model can arise due to the occurrence of bottleneck effects, which may be encountered during the early stage of colonisation of new habitats by invasive species across a wide range of ecological scenarios. As an illustrative example, here we demonstrate the implications of such differences between the two modelling approaches when studying *in silico* the metastatic colonisation of distant organs by cancer cells.

### A. Essentials of the biological problem

Metastasis is a multi-step process that requires cancer cells to leave the primary tumour site, survive in the blood circulation, extravasate and proliferate at distant sites. During the course of such a multifaceted process, cancer cells need to sequentially acquire different phenotypic characteristics and ultimately adapt to the environmental conditions of distant organs, which may be significantly different from those of the primary tumour [41–43].

Cancer cells have been reported to undergo spontaneous, heritable phenotypic variation [44], which may facilitate adaptation to unpredictable environmental changes, such as those faced during the colonisation of a new niche following extravasation [45]. Since metastases are seeded by single cancer cells or small cell clusters, which originate from the primary site, the adaptive process undergone by cancer cells during the early stage of colonisation may be strongly impacted by demographic stochasticity.

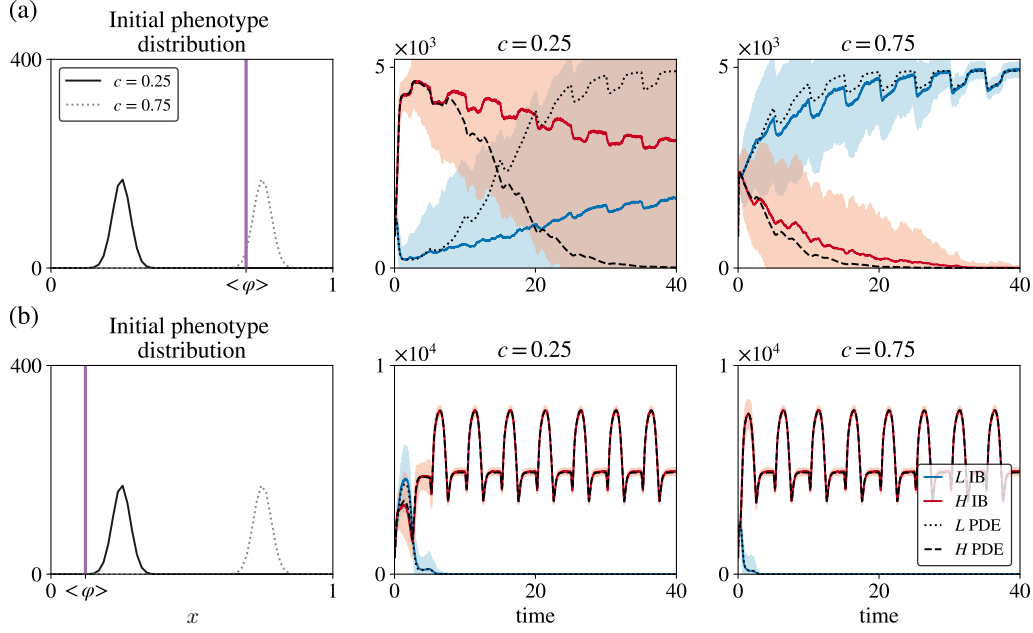


FIG. 7. **Sensitivity analysis of the initial mean phenotype when the nutrient inflow is periodic.** (a) Comparison between numerical simulations of the IB (solid, coloured lines in the central and right panel) and continuum (broken, black lines in the central and right panel) models in the case where the initial phenotype distributions of the two populations are the same and both defined as shown by the plots in the left panel, which correspond to different values of the parameter  $c$  in Eq. (20). The purple line in the first panel highlights the value of the quantity  $\langle \varphi \rangle$  defined according to (22). The evolution of  $S^h$  is governed by the difference equation (11), whereby the term  $I^h$  is defined via Eq. (13) with  $A = 30$  and  $T = 5$ . Numerical simulations are carried out assuming  $a_H = a_L = 800$  and  $b = 1000$  in Eq. (20), and using the parameter values listed in Table I with  $\lambda_H = 0.05$ ,  $\lambda_L = 0.02$  and  $\theta = 10^{-3}$ . The results from the IB model correspond to the average over 30 realisations and the related variance is displayed by the coloured areas surrounding the curves. (b) Same as (a) but for  $\theta = 5 \times 10^{-5}$ .

## B. Definition and calibration of the model

We use the stochastic IB model presented in Section II and its deterministic continuum analogue provided in Section III to investigate the role that spontaneous, heritable phenotypic changes play in the evolutionary dynamics of cancer cells during the early stage of colonisation of a distant organ upon extravasation. In particular, we model the dynamics of cancer cells within a small metastatic lesion that is embedded in a  $1 \text{ mm}^3$  portion of tissue and we assume the metastatic lesion to consist of two competing populations of cancer cells which undergo spontaneous, heritable phenotypic changes with different probabilities.

As before, the population with the lower probability of phenotypic variation is labelled by the index  $L$ , while the other population is labelled by the index  $H$ . Coherently with the existing literature [46], we choose the value of the probability of phenotypic variation  $\lambda_H$  reported in Table II and we estimate the probability of phenotypic variation  $\lambda_L$  to be one order of magnitude smaller than  $\lambda_H$  (*i.e.*  $\lambda_L = 0.1\lambda_H$ ).

In this case, the phenotypic state of every cell at any time  $t_h$  is characterised by the discrete variable  $x_j \in [0, 1]$ , which models the normalised level of ex-

pression of a gene that controls the cell metabolic state, for example, the GLUT-1 gene [47]. In this scenario, cells in the phenotypic state  $x_j = 0$  have a fully oxidative metabolism and produce energy through oxygen consumption only; cells in the phenotypic state  $x_j = 1$  express a fully glycolytic metabolism and produce energy through glucose consumption only; cells in other phenotypic states  $x_j \in (0, 1)$  produce energy via both oxygen and glucose consumption, and higher values of  $x$  correlate with a less oxidative and more glycolytic metabolism [23]. Cells in the phenotypic state  $x_j = 0$  are best adapted to oxygen-rich environments (*i.e.* normoxic conditions), while cells in the phenotypic state  $x_j = 1$  are best adapted to oxygen-poor environments (*i.e.* hypoxic conditions), since they rely on glucose as their primary source of energy and do not require oxygen for their survival. We assume that glucose is not a limiting factor in cancer cell proliferation, since its level remains constantly high [48].

Under the biological scenario corresponding to these assumptions, the parameter  $\gamma$  in our model represents the maximum proliferation rate of fully oxidative phenotypic variants, while the parameter  $\zeta$  is the maximum proliferation rate of fully glycolytic phenotypic variants. Based on the existing literature [49], we estimate the val-

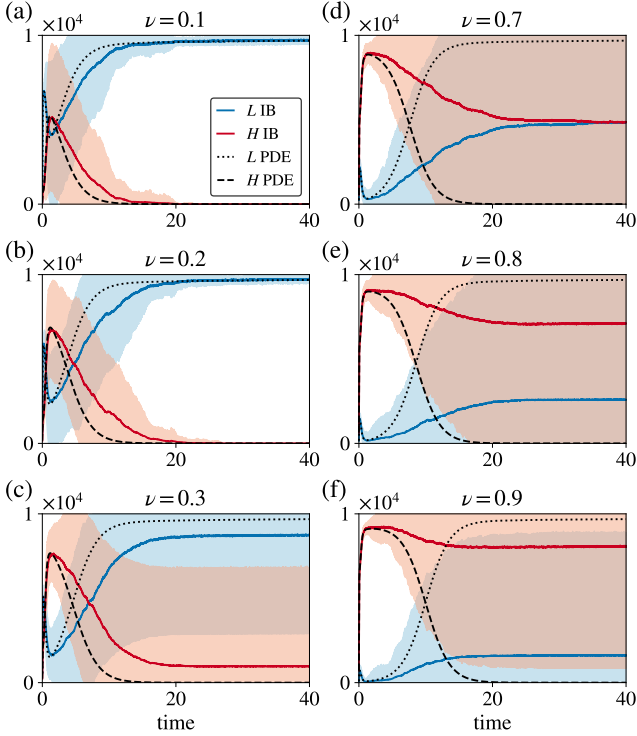


FIG. 8. **Sensitivity analysis of the initial population sizes.** (a) Comparison between numerical simulations of the IB (solid, coloured lines) and continuum (broken, black lines) models in the case where  $a_i$  in Eq. (20) is defined via Eq. (23) with  $Z = 800$  and  $\nu = 0.1$ . The evolution of the nutrient concentration is governed by the difference equation (11), whereby the term  $I^h$  is defined via Eq. (12) with  $\bar{I} = 10$ . Numerical simulations are carried out assuming  $b = 1000$  and  $c = 0.5$  in Eq. (20), and using the parameter values listed in Table I with  $\lambda_H = 0.05$ ,  $\lambda_L = 0.02$  and  $\theta = 10^{-3}$ . The results from the IB model correspond to the average over 30 realisations and the related variance is displayed by the coloured areas surrounding the curves. (b)–(f) Same as (a) but for  $\nu = 0.2$  (panel (b)),  $\nu = 0.3$  (panel (c)),  $\nu = 0.7$  (panel (d)),  $\nu = 0.8$  (panel (e)),  $\nu = 0.9$  (panel (f)).

ues of these parameters to be those reported in Table II. Notice that since glucose is an inefficient energy source compared to oxygen, we have that  $\zeta < \gamma$  [50].

In particular, letting the average diameter of a cell be about  $20 \mu\text{m}$ , we estimate the maximum number of cells that can be accommodated in  $1 \text{ mm}^3$  of tissue to be  $K = 1.25 \times 10^5$  [51], and we assume that only 1% of them can be cancer cells since, during the early stage of metastatic colonisation, other cells that are present in the tissue prior to cancer cell extravasation will leave very limited amount of space available for cancer cells to invade. Hence, using the fact that the approximate carrying capacity for our model in oxygen-rich environments is  $\gamma/d$  [23], we estimate the value of the death rate due

intra- and inter-population competition  $d$  as follows

$$\frac{\gamma}{d} \approx \frac{K}{100} \implies d \approx 100 \frac{\gamma}{K}.$$

We assume the phenotype distributions of the two cell populations at time  $t_h = 0$  to be of the form given by Eq. (20) with the values of the parameters  $a_H$ ,  $a_L$ ,  $b$  and  $c$  corresponding to a biological scenario whereby the two cell populations are both small and mainly composed of cells in the fully oxidative phenotypic state  $x_j = 0$  (cf. the values of the parameters  $a_H$ ,  $a_L$ ,  $b$  and  $c$  reported in Table II).

We let the function  $S^h$  represent the concentration of oxygen available to cancer cells at time  $t_h$ . The dynamic of  $S^h$  is governed by the difference equation (11) whereby the term  $I^h$  models the rate at which cancer cells are supplied with oxygen by blood vessels found in the tissue. Here, the parameter  $\eta$  is the rate of natural decay of oxygen, the value of which is estimated based on [52],  $\kappa$  is the Michaelis constant of oxygen and  $\theta$  is a conversion factor for cell consumption of oxygen, the values of which are chosen consistent with those reported in [49]. Making the simplifying assumption that oxygen supply from blood vessels is constant over time, we define  $I^h$  via Eq. (12). Furthermore, denoting by  $I_v$  the average amount of oxygen released from a single healthy blood vessel, the value of which is chosen based on experimental measurements reported in [53], we use the following definition of the term  $\bar{I}$  in Eq. (12)

$$\bar{I} := \alpha I_v. \quad (24)$$

The parameter  $\alpha > 0$  in Eq. (24) models the level of tissue oxygenation, which is known to be organ-specific – viz. lungs and bones are, respectively, highly- and poorly-oxygenated organs [54].

In summary, the parameter values used to carry out numerical simulations of the IB model are those reported in Table II and the parameter values of the corresponding continuum model are defined accordingly.

### C. Results

We expect lower values of  $\alpha$  in Eq. (24) (i.e. lower levels of tissue vascularisation) to correlate with a lower saturation value of the oxygen concentration. On the basis of the simulation-assisted analysis carried out in [23], we can foresee that lower saturation values of the oxygen concentration will bring about cancer cell populations of smaller size and will favour glycolytic phenotypic variants (i.e. cells in phenotypic states  $x_j \rightarrow 1$ ) over oxidative phenotypic variants (i.e. cells in phenotypic states  $x_j \rightarrow 0$ ). Under the biological conditions corresponding to the initial phenotype distributions considered here (cf. the values of the parameters  $b$  and  $c$  reported in Table II), the initial mean phenotype of the two cancer cell populations is the fully oxidative phenotypic state  $x_j = 0$

TABLE II. Parameter values used in numerical simulations.

Parameter	Value	Units
$\gamma$	0.66	day <sup>-1</sup>
$\zeta$	0.5	day <sup>-1</sup>
$d$	$5.2 \times 10^{-4}$	day <sup>-1</sup> cells <sup>-1</sup>
$K$	$1.25 \times 10^5$	cells
$\theta$	$8.2 \times 10^{-9}$	mmol cells <sup>-1</sup>
$\kappa$	$2.1 \times 10^{-3}$	mmol
$\eta$	0.24	day <sup>-1</sup>
$I_v$	$1.5 \times 10^{-4}$	mmol day <sup>-1</sup>
$\alpha$	{0.01, 1, 10}	—
$\lambda_H$	0.02	—
$\lambda_L$	0.002	—
$a_H, a_L$	25	cells
$b$	1000	—
$c$	0	—
$\tau$	$10^{-3}$	day
$t_f$	365	day
$\chi$	0.032	—

and, therefore, lower values of  $\alpha$  will correspond to initial mean phenotype of lower fitness. Hence, based on the results of the sensitivity analysis presented in Section IV, we expect smaller  $\alpha$  to make it more likely that differences between the IB model and its continuum counterpart will emerge. This is confirmed by the results presented in Figure 9.

The sample dynamics of the size of the cell populations  $H$  and  $L$  displayed in Figure 9 demonstrate that when  $\alpha$  is sufficiently high there is excellent quantitative agreement between the discrete and continuum models (see Figure 9(a)). On the other hand, the match between the two models deteriorates as the value of  $\alpha$  decreases. This discrepancy arises because, in contrast with the deterministic continuum model, the IB model predicts that population  $L$  may be driven to extinction by demographic stochasticity, resulting in the survival of population  $H$  (see Figures 9(b) and 9(c)).

These results communicate the biological notion that higher probabilities of spontaneous, heritable phenotypic changes may constitute a competitive advantage for cancer cells during the early stage of metastatic colonisation of poorly-oxygenated distant organs. The same results act also as a proof of concept for the idea that whilst stochastic effects associated with small cell numbers, which cannot be captured by deterministic continuum models formulated as non-local PDEs, can be, in a first approximation, neglected when modelling the metastatic colonisation of highly-oxygenated distant organs, such as the lungs, they become particularly relevant when considering poorly-oxygenated organs, such as the bones. This supports the idea that particular care should be taken when selecting the mathematical modelling approach employed to describe such a process of biological colonisation of new habitats.

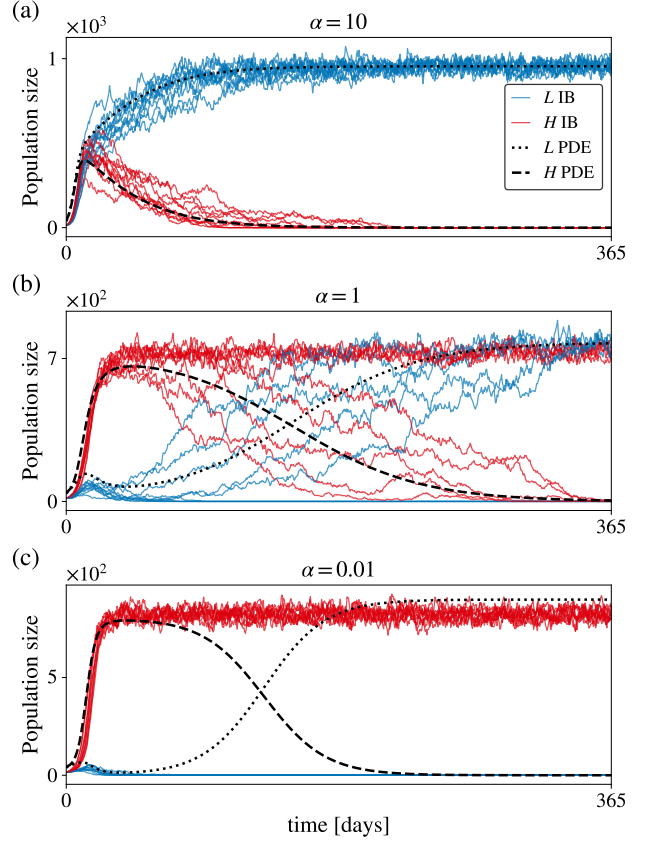


FIG. 9. **Application to the mathematical modelling of metastasis.** (a) Comparison between numerical simulations of the IB (solid, coloured lines) and continuum (broken, black lines) models, in the case where realistic parameter values corresponding to the early stage of metastatic colonisation of distant organs by cancer cells are considered (*cf.* parameter values reported in Table II). The evolution of the oxygen concentration is governed by the difference equation (11) whereby the term  $I^h$  is defined via Eq. (12) and the term  $\bar{I}$  in Eq. (12) is defined according to Eq. (24) with  $\alpha = 10$ . (b), (c) Same as (a) but for  $\alpha = 1$  and  $\alpha = 0.01$ , respectively.

## VI. CONCLUSIONS

We developed a stochastic IB model for the evolutionary dynamics of two competing phenotype-structured cell populations that are exposed to time-varying nutrient levels and undergo spontaneous, heritable phenotypic changes with different probabilities. We formally derived the deterministic continuum counterpart of this model and carried out a systematic comparison between numerical simulations of the IB and continuum models.

We presented base-case results that demonstrate an excellent quantitative match between the outcomes of the two models. These results agree with our previously published analytical and numerical results for related deterministic continuum models [22, 23]. Moreover, we investigated the importance of stochastic effects in driv-

ing differences between the predictions made by the two models and how these cannot be captured by the deterministic continuum model. Finally, considering suitably parameterised versions of the IB and continuum models, we demonstrated how such differences may impact on the mathematical modelling of the early stage of metastatic colonisation of distant organs by cancer cells.

The results obtained indicate that bottleneck effects, which are crucial during the colonisation of new habitats by invasive species, can lead to significant differences between the two models. In fact, more prominent population bottlenecks bring about sharper drops in cell numbers. This correlates with both lower regularity of the density functions of the two populations and more pronounced demographic stochasticity, which cause a reduction in the quality of the approximations employed in the formal derivation of the deterministic continuum model from the stochastic IB model (*cf.* the approximations given by Eqs. (A2)-(A5) and (A7)). In particular, bottleneck effects emerge in the presence of lower probabilities of phenotypic variation, and are more apparent when the two populations are characterised by less fit initial mean phenotypes and smaller initial levels of phenotypic heterogeneity. The emergence of these effects, and thus the agreement between the two modelling approaches, is also dependent on the initial proportions of the two populations.

The generality of our assumptions make the discrete modelling framework considered here applicable to a broad range of asexual organisms exposed to dynamically changing environments. Such a modelling framework, along with the related method to formally derive corresponding continuum models, can be easily extended to incorporate the effects of additional biological aspects related to spatial structure, such as cell movement, inter-cellular spatial interactions, nutrient diffusion and the presence of multiple sources of nutrient distributed across the spatial domain. These extensions will enable a more biologically relevant exploration of the scenarios under which stochastic effects may result in discrepancies between the predictions made by discrete stochastic models and those made by their deterministic continuum limits. This will ultimately help disentangle the impact of, different sources of, stochasticity on the emergence of spatio-temporal evolutionary patterns in a variety of living systems [55, 56].

## ACKNOWLEDGMENTS

AA is supported by funding from the Engineering and Physical Sciences Research Council (EPSRC) and the Medical Research Council (MRC) (grant no. EP/L016044/1) and in part by the Moffitt Cancer Center PSOC, NIH/NCI (grant no. U54CA193489). RG and ARAA are supported by Physical Sciences Oncology Network (PSON) grant from the National Cancer Institute (grant no. U54CA193489) as well as the Cancer Systems

Biology Consortium grant from the National Cancer Institute (grant no. U01CA23238). ARAA and RG would also like to acknowledge support from the Moffitt Cancer Center of Excellence for Evolutionary Therapy. The authors wish to thank the two anonymous Reviewers for their thoughtful feedback on the manuscript.

## Appendix A: Formal derivation of the deterministic continuum model given by the system of non-local PDEs (15)

Using a method analogous to that employed in [32, 33], we show that the coupled system of non-local PDEs (15) can be formally derived as the appropriate continuum limit of our discrete model.

In the case where the dynamics of the cells is governed by the rules described in Section II, the principle of mass balance gives the following difference equations

$$n_{i,j}^{h+1} = \{2\tau p(x_j, S^h) + [1 - \tau(p(x_j, S^h) + d\rho^h)]\} \times \left[ \frac{\lambda_i}{2} n_{i,j+1}^h + \frac{\lambda_i}{2} n_{i,j-1}^h + (1 - \lambda_i) n_{i,j}^h \right],$$

for  $i \in \{H, L\}$ , which can be rewritten as

$$n_{i,j}^{h+1} = (1 + \tau p(x_j, S^h) - \tau d \rho^h) \left[ \frac{\lambda_i}{2} n_{i,j+1}^h + \frac{\lambda_i}{2} n_{i,j-1}^h + (1 - \lambda_i) n_{i,j}^h \right]. \quad (\text{A1})$$

Using the fact that the following relations hold for  $\tau$  and  $\chi$  sufficiently small

$$t_h \approx t, \quad t_{h+1} \approx t + \tau, \quad x_j \approx x, \quad x_{j\pm 1} \approx x \pm \chi,$$

$$n_{i,j}^h \approx n_i(x, t), \quad S^h \approx S(t), \quad (\text{A2})$$

$$n_{i,j}^{h+1} \approx n_i(x, t + \tau), \quad n_{i,j\pm 1}^h \approx n_i(x \pm \chi, t), \quad (\text{A3})$$

$$\rho_i^h \approx \rho_i(t) := \int_0^1 n_i(x, t) dx, \quad (\text{A4})$$

and

$$\rho^h \approx \rho(t) := \int_0^1 n_H(x, t) dx + \int_0^1 n_L(x, t) dx. \quad (\text{A5})$$

Eq. (A1) can be formally rewritten in the approximate form

$$n_i(x, t + \tau) = \left(1 + \tau R(x, S(t), \rho(t))\right) \left[ \frac{\lambda_i}{2} n_i(x + \chi, t) + \frac{\lambda_i}{2} n_i(x - \chi, t) + (1 - \lambda_i) n_i(x, t) \right], \quad (\text{A6})$$



with  $R(x, S(t), \rho(t)) := p(x, S(t)) - d\rho(t)$ . If the function  $n_i(x, t)$  is twice continuously differentiable with respect to the variable  $x$ , for  $\chi$  sufficiently small we can use the Taylor expansions

$$n_i(x \pm \chi, t) = n_i \pm \chi \frac{\partial n_i}{\partial x} + \frac{\chi^2}{2} \frac{\partial^2 n_i}{\partial x^2} + h.o.t., \quad (\text{A7})$$

where  $n_i \equiv n_i(x, t)$ . Substituting Eq. (A7) into Eq. (A6) and dividing both sides of the resulting equation by  $\tau$ , after a little algebra we find

$$\begin{aligned} \frac{n_i(x, t + \tau) - n_i(x, t)}{\tau} &= R(x, S(t), \rho(t)) n_i(x, t) \\ &+ \frac{\lambda_i \chi^2}{2\tau} \frac{\partial^2 n_i(x, t)}{\partial x^2} \\ &+ R(x, S(t), \rho(t)) \frac{\lambda_i \chi^2}{2} \frac{\partial^2 n_i(x, t)}{\partial x^2} + h.o.t. \end{aligned}$$

If, in addition, the function  $n_i(x, t)$  is continuously differentiable with respect to the variable  $t$ , letting  $\tau \rightarrow 0$  and  $\chi \rightarrow 0$  in such a way that the condition given by Eq. (14) is met, from the latter equation we formally obtain

$$\frac{\partial n_i(x, t)}{\partial t} = \beta_i \frac{\partial^2 n_i(x, t)}{\partial x^2} + R(x, S(t), \rho(t)) n_i(x, t),$$

which gives the system of non-local PDEs (15). Finally, the no-flux boundary conditions (16) follow from the fact that the attempted phenotypic variation of a cell is aborted if it requires moving into a phenotypic state that does not belong to the interval  $[0, 1]$ .

## Appendix B: Details of numerical simulations of the continuum model

To construct numerical solutions of the system of non-local PDEs (15) posed on  $(0, 1) \times (0, t_f]$ , and subject both to the no-flux boundary conditions (16) and to the continuum analogue of the initial condition (20), *i.e.*

$$n_i(x, 0) = a_i \left( \frac{b}{2\pi} \right)^{\frac{1}{2}} \exp \left[ -\frac{b}{2} (x - c)^2 \right], \quad (\text{B1})$$

with  $i \in \{H, L\}$ , we use a uniform discretisation of the interval  $(0, 1)$  as the computational domain of the independent variable  $x$ , and we discretise the time interval  $(0, t_f]$  with the uniform step  $\Delta t = 0.0001$ . The method for constructing numerical solutions is based on a three-point finite difference explicit scheme for the diffusion terms and an explicit finite difference scheme for the reaction term [57]. Moreover, the ODE (17), which is subject to the initial condition  $S(0) = 10$  and complemented with the continuum analogues of the alternative definitions of the term  $I^h$  that are specified in the main body of the paper, is solved numerically by using an explicit Euler method with step  $\Delta t$ . Given the values of the param-

eter  $\tau$ ,  $\chi$ ,  $\lambda_H$  and  $\lambda_L$  of the IB model, the values of the parameters  $\beta_H$  and  $\beta_L$  are defined so that the condition given by Eq. (14) is met. The other parameter values are chosen to be coherent with those used to carry out numerical simulations of the IB model, which are specified in the main body of the paper.

## Appendix C: Sample phenotype distributions for the base-case results presented in Section IV A

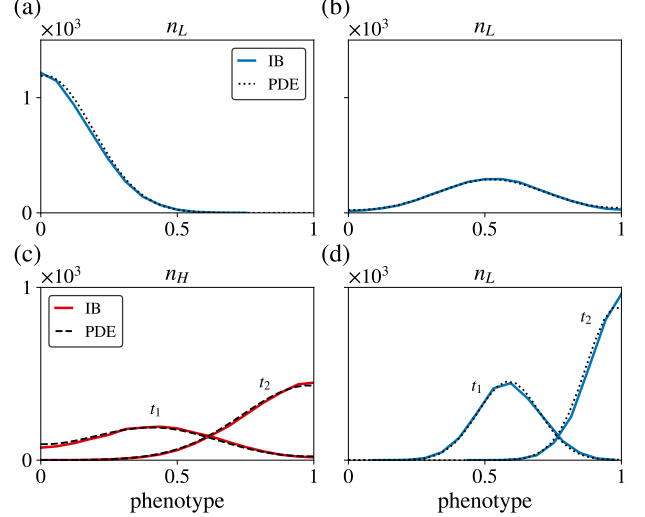


**FIG. 10. Sample phenotype distributions for base-case results.** Comparison between the phenotype distributions of the surviving population for the IB (solid, coloured lines) and continuum (broken, black lines) models in the case where the evolution of the nutrient concentration is governed by the difference equation (11). The results from the IB model correspond to the average over 30 realisations. (a) Phenotype distribution at numerical equilibrium (*i.e.* at time  $t_f = 10$ ) under the simulation set-up of Figure 2(a). (b) Phenotype distribution at numerical equilibrium (*i.e.* at time  $t_f = 10$ ) under the simulation set-up of Figure 2(b). (c) Phenotype distribution at the time instants  $t_1 = 17.5$  and  $t_2 = 20$  under the simulation set-up of Figure 3(a). (d) Phenotype distribution at the time instants  $t_1 = 17.5$  and  $t_2 = 20$  under the simulation set-up of Figure 3(b).

## Appendix D: Base-case results in the case where the nutrient concentration is prescribed

We carried out preliminary numerical simulations in the case where, instead of being the solution of the difference equation (11), the nutrient concentration is prescribed and given by

$$S^h := M + A \sin \left( \frac{2\pi t_h}{T} \right), \quad (\text{D1})$$

where  $M > 0$  is the mean nutrient level, and the parameter  $0 \leq A \leq M$  models the semi-amplitude of possible oscillations of the nutrient level, which have period  $T > 0$ . We fix the values of  $M$  and  $T$  and consider three different values of  $A$  that correspond to distinct environmental regimes: constant nutrient level (*i.e.* no oscillations), mild nutrient fluctuations (*i.e.* small-amplitude oscillations) and severe nutrient fluctuations (*i.e.* large-amplitude oscillations).

The results presented in Figure 11 show that, for all values of  $A$  considered, there is an excellent quantitative match between the numerical simulations of the IB and continuum models. In agreement with the analytical results that we presented in [22], when the nutri-

ent concentration is constant, population  $L$  outcompetes population  $H$  (see Figure 11(a)). The same outcome is observed in the presence of mild nutrient fluctuations (see Figure 11(b)). By contrast, population  $L$  is outcompeted by population  $H$  when severe nutrient fluctuations occur (see Figure 11(c)). In all cases, the phenotype distribution of the surviving population is unimodal and attains its maximum at the mean phenotype (results not shown). Moreover, when the nutrient level is constant, the size and the mean phenotype of the surviving population converge to stable values. On the other hand, in the presence of  $T$ -periodic nutrient fluctuations, the size and mean phenotype of the surviving population converge to  $T$ -periodic functions.

- 
- [1] R. J. Gillies, J. S. Brown, A. R. Anderson, and R. A. Gatenby, Eco-evolutionary causes and consequences of temporal changes in intratumoural blood flow, *Nature Reviews Cancer* **18**, 576 (2018).
  - [2] E. Kussell, R. Kishony, N. Q. Balaban, and S. Leibler, Bacterial persistence: a model of survival in changing environments, *Genetics* **169**, 1807 (2005).
  - [3] C. T. Kremer and C. A. Klausmeier, Coexistence in a variable environment: eco-evolutionary perspectives, *Journal of Theoretical Biology* **339**, 14 (2013).
  - [4] R. Levins, *Evolution in changing environments: some theoretical explorations*, 2 (Princeton University Press, 1968).
  - [5] B. Xue and S. Leibler, Benefits of phenotypic plasticity for population growth in varying environments, *Proceedings of the National Academy of Sciences* **115**, 12745 (2018).
  - [6] K. R. Hopper, Risk-spreading and bet-hedging in insect population biology, *Annual Review of Entomology* **44**, 535 (1999).
  - [7] E. Kussell and S. Leibler, Phenotypic diversity, population growth, and information in fluctuating environments, *Science* **309**, 2075 (2005).
  - [8] T. Philippi and J. Seger, Hedging one's evolutionary bets, revisited, *Trends in Ecology & Evolution* **4**, 41 (1989).
  - [9] J. W. Baron and T. Galla, How successful are mutants in multiplayer games with fluctuating environments? sojourn times, fixation and optimal switching, *Royal Society Open Science* **5**, 172176 (2018).
  - [10] R. Canino-Koning, M. J. Wiser, and C. Ofria, Fluctuating environments select for short-term phenotypic variation leading to long-term exploration, *PLoS Computational Biology* **15** (2019).
  - [11] I. Cvijović, B. H. Good, E. R. Jerison, and M. M. Desai, Fate of a mutation in a fluctuating environment, *Proceedings of the National Academy of Sciences* **112**, E5021 (2015).
  - [12] M. A. Fuentes and E. Ferrada, Environmental fluctuations and their consequences for the evolution of phenotypic diversity, *Frontiers in Physics* **5**, 16 (2017).
  - [13] M. Gómez-Schiavon and N. E. Buchler, Evolutionary dynamics of an epigenetic switch in a fluctuating environment, *bioRxiv*, 072199 (2016).
  - [14] M. Gómez-Schiavon and N. E. Buchler, Epigenetic switching as a strategy for quick adaptation while attenuating biochemical noise, *PLoS Computational Biology* **15** (2019).
  - [15] T. Hiltunen, G. B. Ayan, and L. Becks, Environmental fluctuations restrict eco-evolutionary dynamics in predator-prey system, *Proceedings of the Royal Society B: Biological Sciences* **282**, 20150013 (2015).
  - [16] V. A. Jansen and M. P. Stumpf, Making sense of evolution in an uncertain world, *Science* **309** (2005).
  - [17] S. A. Levin, Population dynamic models in heterogeneous environments, *Annual Review of Ecology and Systematics* **7**, 287 (1976).
  - [18] O. S. Soyer and T. Pfeiffer, Evolution under fluctuating environments explains observed robustness in metabolic networks, *PLoS Computational Biology* **6** (2010).
  - [19] S. D. Tuljapurkar, Population dynamics in variable environments. iii. evolutionary dynamics of r-selection, *Theoretical Population Biology* **21**, 141 (1982).
  - [20] K. Wienand, E. Frey, and M. Mobilia, Eco-evolutionary dynamics of a population with randomly switching carrying capacity, *Journal of The Royal Society Interface* **15**, 20180343 (2018).
  - [21] L. Almeida, P. Bagnerini, G. Fabrini, B. D. Hughes, and T. Lorenzi, Evolution of cancer cell populations under cytotoxic therapy and treatment optimisation: insight from a phenotype-structured model, *ESAIM: Mathematical Modelling and Numerical Analysis* **53**, 1157 (2019).
  - [22] A. Ardaševa, R. A. Gatenby, A. R. Anderson, H. M. Byrne, P. K. Maini, and T. Lorenzi, Evolutionary dynamics of competing phenotype-structured populations in periodically fluctuating environments, *Journal of Mathematical Biology* **80**, 775 (2020).
  - [23] A. Ardaševa, R. A. Gatenby, A. R. A. Anderson, H. M. Byrne, P. K. Maini, and T. Lorenzi, A mathematical dissection of the adaptation of cell populations to fluctuating oxygen levels, *Bulletin of Mathematical Biology* **82**, 81 (2020).
  - [24] C. Carrère and G. Nadin, Influence of mutations in phenotypically-structured populations in time periodic environment, *Discrete & Continuous Dynamical Systems-B* **22**, 0 (2019).
  - [25] S. Figueroa Iglesias and S. Mirrahimi, Long time evolutionary dynamics of phenotypically structured populations in time-periodic environments, *SIAM Journal on*



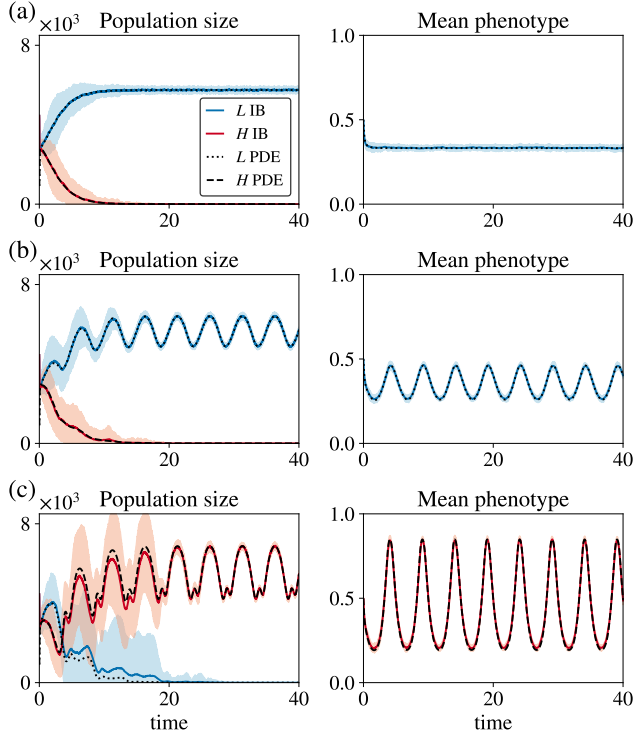


FIG. 11. **Base-case results when the nutrient concentration is prescribed.** Comparison between numerical simulations of the IB (solid, coloured lines) and continuum (broken, black lines) models in the case where the nutrient concentration is prescribed and defined via Eq. (D1). (a) Dynamics of the population sizes (left column) and the mean phenotype of the surviving population (right column) in the case where  $M = 1$ ,  $T = 5$  and  $A = 0$  in Eq. (D1). Here,  $a_H = a_L = 800$ ,  $b = 10$  and  $c = 0.5$  in Eq. (20), and the values of the other parameters are those listed in Table I with  $\lambda_H = 0.05$  and  $\lambda_L = 0.02$ . The results from the IB model correspond to the average over 30 realisations and the related variance is displayed by the coloured areas surrounding the curves. (b)–(c) Same as (a) but for  $A = 0.5$  (row (b)) and  $A = 1$  (row (c)).

Mathematical Analysis **50**, 5537 (2018).

- [26] S. F. Iglesias and S. Mirrahimi, Selection and mutation in a shifting and fluctuating environment, Preprint (2019).
- [27] T. Lorenzi, R. H. Chisholm, L. Desvillettes, and B. D. Hughes, Dissecting the dynamics of epigenetic changes in phenotype-structured populations exposed to fluctuating environments, *Journal of Theoretical Biology* **386**, 166 (2015).
- [28] S. Mirrahimi, B. Perthame, and P. E. Souganidis, Time fluctuations in a population model of adaptive dynamics, *Annales de l'Institut Henri Poincaré (C) Non Linear Analysis* **32**, 41 (2015).
- [29] J. Müller, B. Hense, T. Fuchs, M. Utz, and C. Pötzsche, Bet-hedging in stochastically switching environments, *Journal of Theoretical Biology* **336**, 144 (2013).
- [30] N. Champagnat, R. Ferrière, and S. Méléard, Unifying evolutionary dynamics: from individual stochastic processes to macroscopic models, *Theoretical Population Biology* **69**, 297 (2006).
- [31] N. Champagnat, R. Ferrière, and G. Ben Arous, The canonical equation of adaptive dynamics: a mathematical view, *Selection* **2**, 73 (2002).
- [32] R. H. Chisholm, T. Lorenzi, L. Desvillettes, and B. D. Hughes, Evolutionary dynamics of phenotype-structured populations: from individual-level mechanisms to population-level consequences, *Zeitschrift für Angewandte Mathematik und Physik* **67**, 100 (2016).
- [33] R. E. Stace, T. Stiehl, M. A. Chaplain, A. Marciniak-Czochra, and T. Lorenzi, Discrete and continuum phenotype-structured models for the evolution of cancer cell populations under chemotherapy, *Mathematical Modelling of Natural Phenomena* **15**, 14 (2020).
- [34] D. A. Chan and A. J. Giaccia, Hypoxia, gene expression, and metastasis, *Cancer and Metastasis Reviews* **26**, 333 (2007).
- [35] B. D. Hughes, *Random walks and random environments: random walks*, Vol. 1 (Oxford University Press, 1995).
- [36] S. Huang, Genetic and non-genetic instability in tumor progression: link between the fitness landscape and the epigenetic landscape of cancer cells, *Cancer and Metastasis Reviews* **32**, 423 (2013).
- [37] J. Hereford, A quantitative survey of local adaptation and fitness trade-offs, *The American Naturalist* **173**, 579 (2009).
- [38] D. Basanta, M. Simon, H. Hatzikirou, and A. Deutsch, Evolutionary game theory elucidates the role of glycolysis in glioma progression and invasion, *Cell Proliferation* **41**, 980 (2008).
- [39] R. R. Bravo, E. Baratchart, J. West, R. O. Schenck, A. K. Miller, J. Gallaher, C. D. Gatenbee, D. Basanta, M. Robertson-Tessi, and A. R. Anderson, Hybrid automata library: A flexible platform for hybrid modeling with real-time visualization, *PLOS Computational Biology* **16**, e1007635 (2020).
- [40] S. H. Rice, *Evolutionary theory: mathematical and conceptual foundations* (Sinauer Associates, 2004).
- [41] J. Massagué and A. C. Obenauf, Metastatic colonization by circulating tumour cells, *Nature* **529**, 298 (2016).
- [42] A. C. Obenauf and J. Massagué, Surviving at a distance: organ-specific metastasis, *Trends in cancer* **1**, 76 (2015).
- [43] N. Sethi and Y. Kang, Unravelling the complexity of metastasis? molecular understanding and targeted therapies, *Nature Reviews Cancer* **11**, 735 (2011).
- [44] P. B. Gupta, C. M. Fillmore, G. Jiang, S. D. Shapira, K. Tao, C. Kuperwasser, and E. S. Lander, Stochastic state transitions give rise to phenotypic equilibrium in populations of cancer cells, *Cell* **146**, 633 (2011).
- [45] M. K. Jolly, P. Kulkarni, K. Weninger, J. Orban, and H. Levine, Phenotypic plasticity, bet-hedging, and androgen independence in prostate cancer: Role of non-genetic heterogeneity, *Frontiers in oncology* **8**, 50 (2018).
- [46] T. Lorenzi, R. H. Chisholm, and J. Clairambault, Tracking the evolution of cancer cell populations through the mathematical lens of phenotype-structured equations, *Biology direct* **11**, 43 (2016).
- [47] R. Gatenby, K. Smallbone, P. Maini, F. Rose, J. Averill, R. B. Nagle, L. Worrall, and R. Gillies, Cellular adaptations to hypoxia and acidosis during somatic evolution of breast cancer, *British journal of cancer* **97**, 646 (2007).
- [48] C. A. Gravenmier, M. Siddique, and R. A. Gatenby, Adaptation to stochastic temporal variations in intratumoral blood flow: the warburg effect as a bet hedge-

- ing strategy, *Bulletin of mathematical biology* **80**, 954 (2018).
- [49] J. J. Casciari, S. V. Sotirchos, and R. M. Sutherland, Variations in tumor cell growth rates and metabolism with oxygen concentration, glucose concentration, and extracellular ph, *Journal of cellular physiology* **151**, 386 (1992).
  - [50] M. G. Vander Heiden, L. C. Cantley, and C. B. Thompson, Understanding the warburg effect: the metabolic requirements of cell proliferation, *Science* **324**, 1029 (2009).
  - [51] R. H. Chisholm, T. Lorenzi, A. Lorz, A. K. Larsen, L. N. de Almeida, A. Escargueil, and J. Clairambault, Emergence of drug tolerance in cancer cell populations: an evolutionary outcome of selection, nongenetic instability, and stress-induced adaptation, *Cancer research* **75**, 930 (2015).
  - [52] P. Cumsille, A. Coronel, C. Conca, C. Quiñinao, and C. Escudero, Proposal of a hybrid approach for tumor progression and tumor-induced angiogenesis, *Theoretical biology and medical modelling* **12**, 13 (2015).
  - [53] A. G. Tsai, B. Friesenecker, M. C. Mazzoni, H. Kerger, D. G. Buerk, P. C. Johnson, and M. Intaglietta, Microvascular and tissue oxygen gradients in the rat mesentery, *Proceedings of the National Academy of Sciences* **95**, 6590 (1998).
  - [54] A. Carreau, B. E. Hafny-Rahbi, A. Matejuk, C. Grillon, and C. Kieda, Why is the partial oxygen pressure of human tissues a crucial parameter? small molecules and hypoxia, *Journal of cellular and molecular medicine* **15**, 1239 (2011).
  - [55] M. Robertson-Tessi, R. J. Gillies, R. A. Gatenby, and A. R. Anderson, Impact of metabolic heterogeneity on tumor growth, invasion, and treatment outcomes, *Cancer Research* **75**, 1567 (2015).
  - [56] W. Thuiller, J. A. Slingsby, S. D. Privett, and R. M. Cowling, Stochastic species turnover and stable coexistence in a species-rich, fire-prone plant community, *PLoS One* **2** (2007).
  - [57] R. J. LeVeque, *Finite difference methods for ordinary and partial differential equations: steady-state and time-dependent problems* (Society for Industrial and Applied Mathematics (SIAM), Philadelphia, 2007).